ISSN 2616-5775 Vol. 9, Issue 7: 75-83, DOI: 10.25236/AJCIS.2026.090710

Protection-Aware Electro-Thermal Modeling for Smartphone Battery Time-to-Empty Prediction

Xi Cao[1,a,*], Weihao Dong[1,b], Lihao Zhang[1,c]

[1]*Brunel College, North China University of Technology, Beijing, 100144, China*
[a]*18641884633@163.com*, [b]*skyshin34@163.com*, [c]*1975822067@qq.com*
**Corresponding author*

Abstract: *Accurate smartphone time-to-empty (TTE) prediction cannot be obtained by extrapolating state of charge (SOC) alone. Near low SOC, under high load, at low temperature, or after battery aging, terminal-voltage sag and increased internal resistance may make demanded power infeasible before stored charge is depleted. This paper presents a compact protection-aware electro-thermal framework for TTE prediction from smartphone usage logs. The framework follows one engineering chain: usage logs are reconstructed as a continuous demanded-power trajectory, demanded power is closed through an electro-thermal battery model, the deliverability margin drives runtime throttling and undervoltage protection, and TTE is computed as the first infeasible operating time. The model addresses two research questions: how usage logs can be transformed into $P_{dem}(t)$, and how deliverability constraints and operating-system protection improve realistic TTE prediction. The formulation combines interpretable demand reconstruction, OCV/internal-resistance power closure, SOC and thermal dynamics, aging-dependent capacity and resistance, soft power clipping, and UVLO-based shutdown. It explains non-zero SOC shutdown and provides a physics-constrained basis for evaluating runtime under different loads, temperatures, and aging states.*

Keywords: *time-to-empty prediction; electro-thermal battery model; deliverability limit; protection-aware modeling; voltage sag; runtime throttling; non-zero SOC shutdown; battery feasibility*

1. Introduction

Smartphone TTE is often estimated from SOC and recent discharge rate. This approximation is acceptable during mild operation, but it fails near the edge of battery feasibility. A device can still report nonzero SOC and yet lose power when a high instantaneous workload causes terminal voltage to fall below the stable operating range. This behavior is especially common under cold temperature, high CPU or radio load, and aged batteries with increased internal resistance.

The key engineering issue is power deliverability. Stored charge describes remaining energy, whereas deliverability describes whether the battery can supply the requested power without violating voltage, thermal, or protection constraints. Voltage sag increases with current and internal resistance [1]. Aging reduces effective capacity and increases resistance. Temperature changes resistance and heat dissipation. The operating system then enforces protection through runtime throttling, power clipping, and undervoltage lockout (UVLO).

Prior smartphone power models usually decompose consumption into display, processor, radio, location, and background-service components, while battery-management studies provide the equivalent-circuit and state-estimation foundations used here [2]. Display models distinguish backlight-driven LCD power from content-dependent OLED power, and processor models often use workload and frequency proxies for DVFS behavior. Electro-thermal battery models, in contrast, represent voltage response, internal resistance, SOC evolution, and heat generation; their parameter identification and state-estimation variants motivate the closure adopted in this paper [3] [4]. These two streams are complementary: demand models explain what the phone requests, while electro-thermal and equivalent-circuit comparisons determine whether the battery can deliver it [5].

Existing TTE predictors include moving-average extrapolation, empirical discharge fitting, data-driven sequence models, and model-based estimators for SOC, SOH, and state-of-available-power prediction [6] [7]. Aging studies further show that capacity loss and resistance growth must be considered when predicting runtime near the feasible-power boundary [8] [9]. Empirical and data-driven predictors can work in familiar regimes, but they often lack explicit battery feasibility constraints. Protection behaviors such as UVLO, thermal cutoff, cold-temperature power limitation, and runtime throttling are therefore frequently treated as anomalies rather than as part of the TTE mechanism [10]. This paper integrates these behaviors into the prediction model, drawing on battery monitoring, SOH estimation, state-of-available-power prediction, combined SOC/SOH estimation, and cold-temperature battery analyses [11] [12] [13] [14] [15].

The study is organized around two research questions. RQ1 asks how smartphone usage logs can be transformed into a continuous power-demand trajectory. RQ2 asks how electro-thermal deliverability constraints and OS protection mechanisms can improve realistic TTE prediction. The contributions are an interpretable usage-log-based $P_{dem(t)}$ reconstruction, a physics-constrained electro-thermal power closure, and a protection-aware TTE definition that explains non-zero SOC shutdown. The complete modeling workflow, from usage-log reconstruction to protection-aware TTE prediction, is summarized in Figure 1.

Protection-Aware Electro-Thermal TTE Prediction Workflow

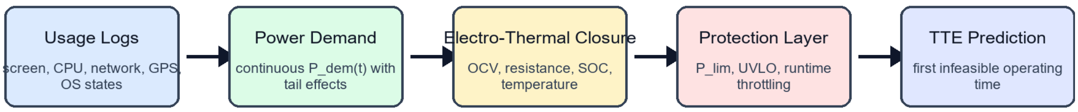

Figure 1 Proposed workflow from usage logs to protection-aware TTE prediction.

2. Methodology

2.1. Problem Formulation

Let t denote time in seconds. The battery state is $x_{(t)} = [z(t), V(t), I(t), T_b(t), SOH]^T$, where z is SOC, V is terminal voltage, I is discharge current, T_b is battery temperature, and SOH is state of health. The synchronized usage log vector $u(t)$ contains screen, CPU, memory, network, GPS, background, and OS-state variables. TTE is defined as the earliest stopping time among SOC depletion, electrical infeasibility, and thermal protection. In the compact source formulation, this is written as:

$$TTE=\min\{\tau_S,\tau_E,\tau_T\} \tag{1}$$

Here τ_S denotes the SOC-depletion stopping time, τ_E denotes the electrical feasibility or voltage-protection stopping time, and τ_T denotes the thermal-protection stopping time. This definition separates demanded power $P_{dem}(t)$, requested by applications and system activity, from deliverable power $P_{del}(t)$, allowed by the battery and protection layer.

2.2. Usage-Log-Based Power Demand Reconstruction

Raw logs are cleaned, unit-normalized, and resampled onto a 1 Hz timeline. Charging intervals and nonphysical telemetry points are removed. Discharge episodes are extracted using charge status and current direction. Continuous variables are standardized within device or episode when needed, and event variables are held piecewise constant between observations. Intervals near protection or shutdown are flagged and not used to identify the unconstrained demand model.

The engineered feature vector contains screen intensity, CPU load, memory activity, network traffic and signal quality, GPS state, background-service activity, and OS switches. LCD display power is treated as brightness/backlight dependent, while OLED power is treated as luminance and content dependent. CPU and memory proxies reflect workload and DVFS behavior. Network power combines data rate with a weak-signal penalty.

The demanded-power model is formulated as

$$P_{\mathrm{dem}}(t)=P_0+\sum_{k\in K} P_k\left(\widetilde{u_k}(t)\right)+P_{\mathrm{res}}(t) \tag{2}$$

The component powers are nonnegative and monotone in their corresponding intensity variables.

ISSN 2616-5775 Vol. 9, Issue 7: 75-83, DOI: 10.25236/AJCIS.2026.090710

Representative module forms are

$$P_{\mathrm{scr,LCD}}(t)=\alpha_{\mathrm{LCD}}\cdot A\cdot L(t)\cdot\left(\frac{f_{\mathrm{scr}}}{60}\right)^{\gamma_{\mathrm{LCD}}} \tag{3}$$

$$P_{\mathrm{cpu}}(t)=f_{\mathrm{cpu}}\left(u_{\mathrm{cpu}}(t)\right), P_{\mathrm{mem}}(t)=f_{\mathrm{mem}}\left(u_{\mathrm{mem}}(t)\right), f'(\cdot)\geq 0 \tag{4}$$

$$P_{\mathrm{net}}(t)=f_{\mathrm{net}}\left(u_{\mathrm{tx/rx}}(t)\right)\cdot\phi\left(q(t)\right),\phi'(\cdot)\leq 0 \tag{5}$$

Post-activity consumption is represented by a first-order tail state, which captures radio residency, delayed synchronization, and DVFS settling:

$$\dot{z}_k(t)=\frac{u_k(t)-z_k(t)}{\tau_k},\widetilde{u_k}(t)=z_k(t),k\in K_{\mathrm{tail}} \tag{6}$$

The parameters are estimated on non-throttled segments by matching measured battery-side power $P_{\mathrm{meas}}(t) = V(t)I(t)$. The output of this stage is $P_{dem}(t)$, together with module-level energy shares and tail-energy contributions. The resulting component-wise energy shares for LED/LCD and OLED episodes are summarized in Figure 2. The contribution of individual demand modules is further assessed by ablation analysis, as shown in Figure 3.

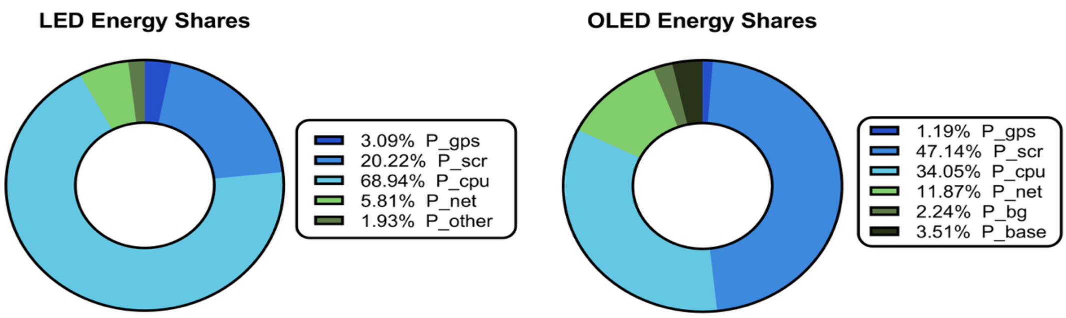

Figure 2 Component-wise power-demand reconstruction for LED/LCD and OLED episodes.

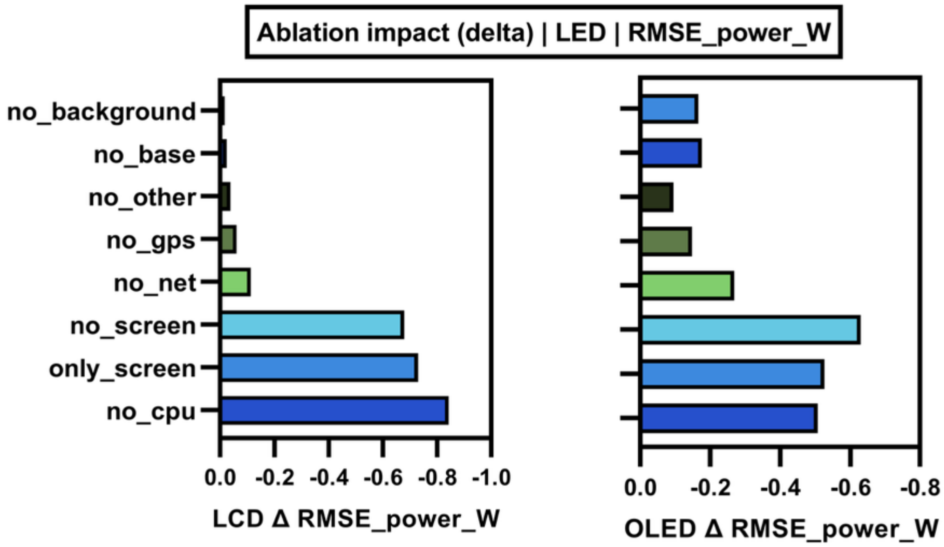

Figure 3 Ablation validation of reconstructed power demand using RMSE increase after module removal.

ISSN 2616-5775 Vol. 9, Issue 7: 75-83, DOI: 10.25236/AJCIS.2026.090710

2.3. Electro-Thermal Power Closure Model

The demand layer estimates what the phone requests. The electro-thermal layer determines whether the battery can deliver it. Terminal voltage is represented by an internal-resistance equivalent model, following common equivalent-circuit battery modeling practice:

$$V(t)=\mathrm{OCV}\big(S(t),T_b(t)\big)-I(t)R\big(S(t),T_b(t)\big) \tag{7}$$

Battery-side power is therefore

$$P_{\mathrm{act}}(t)=V(t)\,I(t) \tag{8}$$

For a requested deliverable power, the physically consistent discharge current is

$$R\,I^2-\mathrm{OCV}\,I+P_{\mathrm{act}}=0 \tag{9}$$

This expression is valid only if the discriminant is nonnegative:

$$\Delta(t)=\mathrm{OCV}^2(S,T_b)-4\,R(S,T_b)\,P_{\mathrm{act}}(t)\geq 0 \tag{10}$$

The unconstrained electrical maximum is

$$P_{\mathrm{feas}}(S,T_b)=\frac{\mathrm{OCV}^2(S,T_b)}{4\,R(S,T_b)} \tag{11}$$

The UVLO threshold imposes a stricter operating limit:

$$P_{\mathrm{uvlo}}(S,T_b)=\frac{V_{\min}\big(\mathrm{OCV}(S,T_b)-V_{\min}\big)}{R(S,T_b)} \tag{12}$$

SOC evolves by Coulomb counting with aging-adjusted capacity:

$$\frac{dS}{dt}=-\frac{I(t)}{Q_{\mathrm{eff}}(T_b,a)} \tag{13}$$

Thermal dynamics are modeled using a lumped heat balance derived from classical battery energy-balance theory and compact thermal models:

$$C_{\mathrm{th}}\frac{dT_b}{dt}=\eta\,I^2R(S,T_b)-\mathrm{h}(T_b-T_{\mathrm{amb}}) \tag{14}$$

Aging is represented by capacity fade and resistance growth, consistent with calendar/cycle aging studies and SOH reviews:

$$P_{\mathrm{res}}(t)\geq 0 \tag{15}$$

Equations (7)-(15) close the loop from demanded power to current, voltage, temperature, and SOC. They also define the deliverability limit used by the protection layer. The corresponding electro-thermal response under different load tiers, including heating trajectories and temperature distributions, is illustrated in Figure 4.

ISSN 2616-5775 Vol. 9, Issue 7: 75-83, DOI: 10.25236/AJCIS.2026.090710

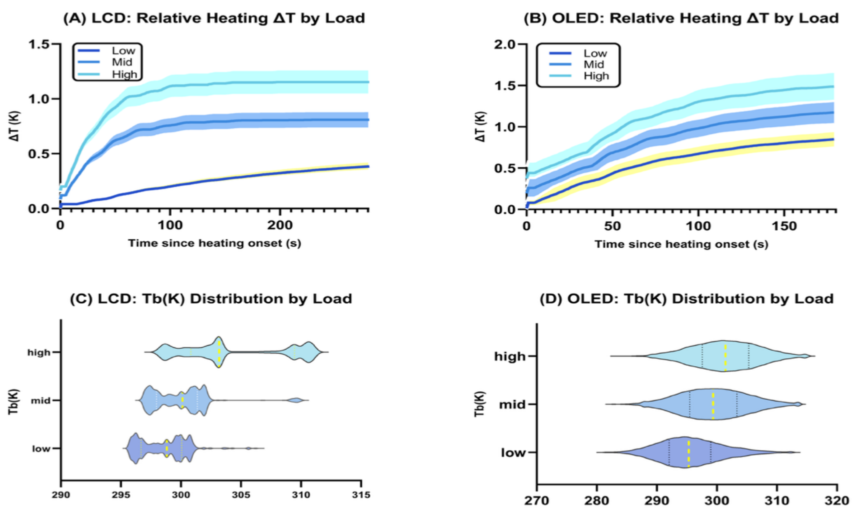

Figure 4 Electro-thermal response validation under load tiers using heating trajectories and temperature distributions.

2.4. Protection and Throttling-Aware TTE Prediction

Runtime protection is modeled as a state-dependent power envelope. The available power limit and instantaneous power margin are

$$P_{\text{lim}}(S,T_b)=\min\{P_{\text{feas}}(S,T_b),\ P_{\text{uvlo}}(S,T_b)\} \tag{16}$$

$$\delta(t)=P_{\text{lim}}\big(S(t),T_b(t)\big)\text{-}P_{\text{dem}}(t) \tag{17}$$

If $m(t)$ is nonnegative, the demanded power is feasible. If $m(t)$ is negative, the OS reduces workload through runtime throttling. A smooth clipping form avoids discontinuous hard switching:

$$g(t)=\sigma\big(\kappa\,\delta(t)\big)=\frac{1}{1+\exp\big(\text{-}\kappa\,\delta(t)\big)} \tag{18}$$

$$P_{\text{act}}(t)=g(t)\ P_{\text{dem}}(t)+\big(1\text{-}g(t)\big)\ P_{\text{lim}}\big(S(t),T_b(t)\big) \tag{19}$$

The quantity $1\text{-}g(t)$ is the throttling severity. Protection-aware TTE is the earliest of SOC depletion, thermal cutoff, UVLO violation, or unsustainable throttling:

$$\tau_S=\inf\{\ t{:}\ S(t)\leq S_{mi}\ \} \tag{20}$$

$$\tau_R=\inf\{\ t{:}\ V(t)<V_{min}\ \text{ or }\ g(t)\leq g_{min}\ \} \tag{21}$$

This formulation explicitly models non-zero SOC shutdown by linking available power prediction, voltage limits, and protection thresholds. Shutdown occurs before $z(t)$ reaches zero when voltage sag, internal resistance, aging, cold temperature, or load peaks shrink $P_{\text{lim}}(t)$ below the minimum sustainable operating power. The device may first throttle and then shut down once UVLO or severe clipping is reached. Figure 5 schematically summarizes this protection-aware throttling process and the mechanism leading to non-zero SOC shutdown.

ISSN 2616-5775 Vol. 9, Issue 7: 75-83, DOI: 10.25236/AJCIS.2026.090710

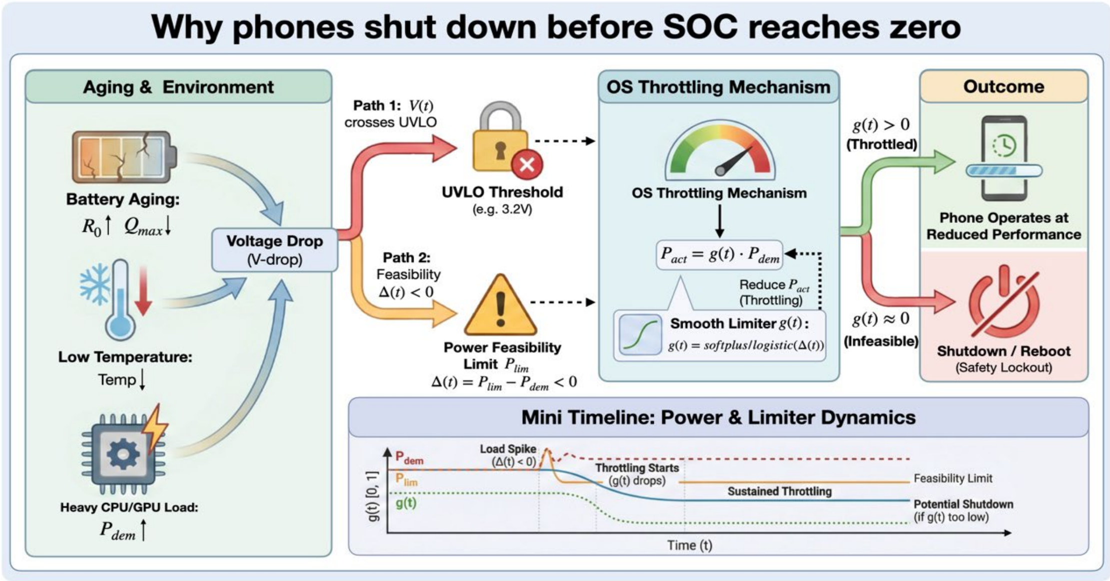

Figure 5 Protection-aware throttling and non-zero SOC shutdown mechanism.

2.5. Experimental Setup

The experimental data include smartphone usage logs and battery telemetry: SOC, voltage, current, temperature, brightness, CPU activity, network traffic, GPS state, and OS switches. All variables are aligned to a common timeline. Discharge episodes are extracted by removing charging intervals and filtering implausible voltage, current, SOC, or temperature values.

Episodes are labeled by load level, display type, aging state when available, and proximity to protection events. Session-level and device-level splits are used where possible. The training set estimates model parameters, the validation set selects smoothing and soft-clipping hyperparameters, and the test set reports final performance. Heating transients, discharge episodes, and shutdown events are kept intact across splits to avoid leakage.

Demand reconstruction is evaluated using power RMSE and integrated energy error. Electro-thermal validation uses SOC, voltage, and temperature trajectory errors. TTE prediction is evaluated using absolute error, relative error, and shutdown-mode agreement. Non-zero SOC shutdown is evaluated by checking whether the predicted stopping mode matches observed protection or shutdown behavior.

3. Results and Discussion

3.1. Power Demand Reconstruction Accuracy

Figure 2 shows that the demand layer produces interpretable component shares. LED/LCD episodes are more CPU dominated, while OLED episodes shift a larger fraction toward screen power. Figure 3 shows that removing CPU or screen modules causes the largest increase in power RMSE, confirming that these terms are structurally necessary for reconstructing $P_{dem}(t)$.

3.2. SOC, Voltage, and Temperature Validation

The electro-thermal model produces realistic state trajectories under different loads. Figure 4 shows that heating increases with load and follows a saturating first-order trend, supporting the lumped thermal balance used in the closure model. The SOC trajectory validation across low, medium, and high load conditions is presented in Figure 6.

ISSN 2616-5775 Vol. 9, Issue 7: 75-83, DOI: 10.25236/AJCIS.2026.090710

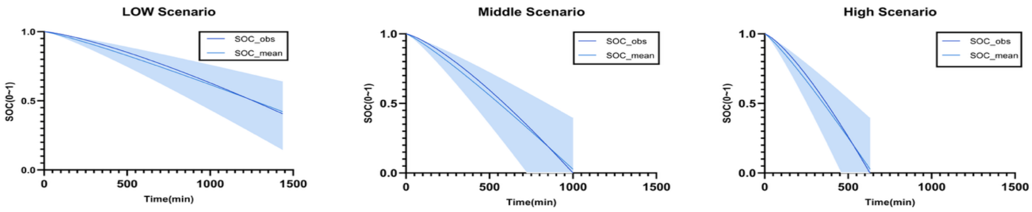

Figure 6 SOC trajectory validation under low, medium, and high load.

Figure 6 shows that the predicted SOC trajectory tracks the observed trend across load regimes. The high-load case reaches the terminal regime earlier, and uncertainty grows near the end of discharge because small changes in resistance, OCV, and protection thresholds are amplified near the feasibility boundary.

3.3. TTE Prediction under Loads and Aging

Figure 7 reports TTE as a function of initial *SOC*, load, and aging. Higher initial *SOC* increases runtime, but the relationship depends strongly on load and *SOH*. Heavy load shortens TTE by increasing $P_{dem}(t)$ and by accelerating thermal and voltage effects. Aging shortens TTE by reducing Q_{eff} and increasing R, which compresses $P_{lim}(t)$ and triggers throttling or shutdown earlier.

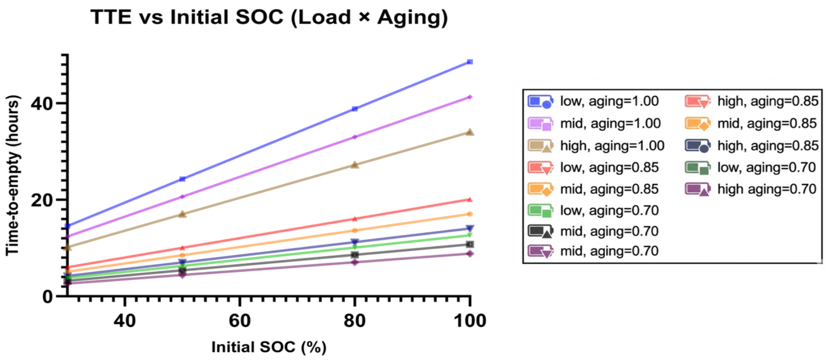

Figure 7 Protection-aware TTE prediction under different initial SOC, load, and aging conditions.

3.4. Non-Zero SOC Shutdown Analysis

Non-zero SOC shutdown is explained by the mismatch between demanded and deliverable power. A SOC-only predictor assumes that the phone remains usable until $z(t)$ approaches zero. The proposed model instead stops when the protection-aware TTE condition is triggered. When aging, cold temperature, or heavy load reduces $P_{lim}(t)$, the power margin $m(t)$ becomes negative. The OS may reduce Pact(t) through $g(t)$, but shutdown occurs if *UVLO* is reached or if the required throttling is too severe to sustain operation.

This mechanism explains abrupt shutdown at positive SOC without treating it as measurement noise. It also explains why a phone can sometimes linger at low SOC under light load, yet shut down at a higher SOC under a sudden CPU, display, or radio peak. The deciding variable is not SOC alone, but the battery feasibility margin.

3.5. Sensitivity Analysis

Sensitivity analysis perturbs each parameter block around its calibrated value and records the resulting change in TTE, peak temperature, and shutdown mode. Figure 8 shows that effective capacity and electrical deliverability parameters have the largest effect on TTE. CPU demand and power-limiting thresholds are also important in overload regimes, while thermal parameters mainly act through sustained-load feedback.

ISSN 2616-5775 Vol. 9, Issue 7: 75-83, DOI: 10.25236/AJCIS.2026.090710

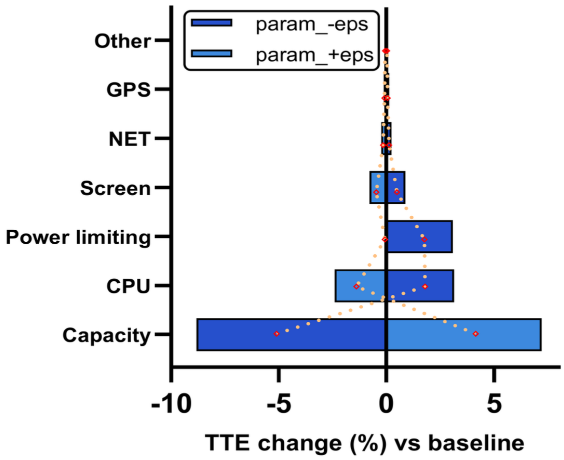

Figure 8 Sensitivity analysis of TTE with respect to demand, capacity, and power-limiting parameters.

The sensitivity results support the model hierarchy. Demand features determine $P_{dem}(t)$. Electro-thermal parameters determine $P_{lim}(t)$. Protection thresholds determine whether overload becomes throttling or shutdown. The strongest uncertainty near early shutdown therefore lies in resistance, capacity, OCV, and UVLO-related parameters.

4. Conclusion

In this study, a protection-aware electro-thermal framework for smartphone time-to-empty (TTE) prediction was developed by coupling usage-log-driven power-demand reconstruction with battery deliverability constraints and operating-system protection behavior. Unlike conventional SOC-based runtime estimation approaches, the proposed framework explicitly distinguishes between stored charge and deliverable power, thereby enabling physically consistent prediction of runtime degradation, throttling, and premature shutdown under high-load, low-temperature, and aged-battery conditions.

The proposed methodology addressed two key research questions. First, smartphone usage logs were transformed into a continuous demanded-power trajectory through interpretable module-level reconstruction involving screen activity, CPU workload, memory behavior, network conditions, GPS usage, and post-activity tail dynamics. Second, the demanded power was closed through an electro-thermal battery model incorporating voltage response, internal resistance, thermal evolution, aging-dependent capacity fade, and undervoltage protection constraints. This closure established a dynamic feasibility boundary between requested and physically deliverable power.

The results demonstrated that runtime prediction near the terminal operating regime is governed not only by SOC depletion, but also by the interaction among voltage sag, resistance growth, thermal feedback, and protection thresholds. In particular, the framework provided a physically interpretable explanation for non-zero SOC shutdown, showing that abrupt device power loss can emerge when the demanded power exceeds the feasible operating envelope even though residual charge remains available. The protection-aware throttling formulation further captured the continuous transition from feasible operation to constrained runtime behavior, avoiding unrealistic hard-switch assumptions.

Sensitivity analysis indicated that effective capacity, internal resistance, and power-limiting thresholds dominate TTE uncertainty near early shutdown conditions, whereas thermal parameters mainly influence sustained-load behavior through cumulative heating effects. These findings suggest that accurate runtime prediction for modern smartphones requires simultaneous consideration of user behavior, electro-thermal battery dynamics, and embedded protection logic rather than relying solely on discharge extrapolation.

The proposed framework remains compact and computationally interpretable, making it potentially suitable for lightweight deployment in battery-management and runtime-estimation systems. Nevertheless, several limitations remain. The present study adopts a reduced-order electro-thermal representation and does not yet incorporate detailed electrochemical diffusion effects, adaptive user-behavior prediction, or device-specific operating-system scheduling strategies. Future work will therefore focus on integrating online parameter adaptation, data-driven workload forecasting, and cross-device transferability analysis under real-world operating conditions.

ISSN 2616-5775 Vol. 9, Issue 7: 75-83, DOI: 10.25236/AJCIS.2026.090710

References

[1] Bernardi, D., Pawlikowski, E. and Newman, J. (1985) A General Energy Balance for Battery Systems. Journal of The Electrochemical Society, 132, 5-12.

[2] Plett, G.L. (2004). Extended Kalman Filtering for Battery Management Systems of LiPB-Based HEV Battery Packs. Part 1. Background. Journal of Power Sources, 134, 252-261.

[3] Plett, G.L. (2004). Extended Kalman Filtering for Battery Management Systems of LiPB-Based HEV Battery Packs. Part 2. Modeling and Identification. Journal of Power Sources, 134, 262-276.

[4] Plett, G.L. (2004). Extended Kalman Filtering for Battery Management Systems of LiPB-Based HEV Battery Packs. Part 3. State and Parameter Estimation. Journal of Power Sources, 134, 277-292.

[5] Hu, X., Li, S. and Peng, H. (2012) A Comparative Study of Equivalent Circuit Models for Li-Ion Batteries. Journal of Power Sources, 198, 359-367.

[6] Forgez, C., Vinh Do, D., Friedrich, G., Morcrette, M. and Delacourt, C. (2010) Thermal Modeling of a Cylindrical LiFePO4/Graphite Lithium-Ion Battery. Journal of Power Sources, 195, 2961-2968.

[7] Lin, X., Perez, H.E., Mohan, S., Siegel, J.B., Stefanopoulou, A.G., Ding, Y. and Castanier, M.P. (2014) A Lumped-Parameter Electro-Thermal Model for Cylindrical Batteries. Journal of Power Sources, 257, 1-11.

[8] Ecker, M., Nieto, N., Kaebitz, S., Schmalstieg, J., Blanke, H., Warnecke, A. and Sauer, D.U. (2014) Calendar and Cycle Life Study of Li(NiMnCo)O2-Based 18650 Lithium-Ion Batteries. Journal of Power Sources, 248, 839-851.

[9] Schmalstieg, J., Kaebitz, S., Ecker, M. and Sauer, D.U. (2014) A Holistic Aging Model for Li(NiMnCo)O2-Based 18650 Lithium-Ion Batteries. Journal of Power Sources, 257, 325-334.

[10] Lu, L., Han, X., Li, J., Hua, J. and Ouyang, M. (2013) A Review on the Key Issues for Lithium-Ion Battery Management in Electric Vehicles. Journal of Power Sources, 226, 272-288.

[11] Waag, W., Fleischer, C. and Sauer, D.U. (2014) Critical Review of the Methods for Monitoring of Lithium-Ion Batteries in Electric and Hybrid Vehicles. Journal of Power Sources, 258, 321-339.

[12] Berecibar, M., Gandiaga, I., Villarreal, I., Omar, N., Van Mierlo, J. and Van den Bossche, P. (2016) Critical Review of State of Health Estimation Methods of Li-Ion Batteries for Real Applications. Renewable and Sustainable Energy Reviews, 56, 572-587.

[13] Farmann, A. and Sauer, D.U. (2016) A Comprehensive Review of On-Board State-of-Available-Power Prediction Techniques for Lithium-Ion Batteries in Electric Vehicles. Journal of Power Sources, 329, 123-137.

[14] Zou, Y., Hu, X., Ma, H. and Li, S.E. (2015) Combined State of Charge and State of Health Estimation over Lithium-Ion Battery Cell Cycle Lifespan for Electric Vehicles. Journal of Power Sources, 273, 793-803.

[15] Jaguemont, J., Boulon, L. and Dube, Y. (2016) A Comprehensive Review of Lithium-Ion Batteries Used in Hybrid and Electric Vehicles at Cold Temperatures. Applied Energy, 164, 99-114.